IEEE Access
Multidisciplinary ⋮ Rapid Review ⋮ Open Access Journal

Received February 7, 2020, accepted March 11, 2020, date of publication March 18, 2020, date of current version March 27, 2020.

Digital Object Identifier 10.1109/ACCESS.2020.2981595

Resonant Converter for Battery Charging Applications With CC/CV Output Profiles

SHUCHANG WANG[1,2], YUSHEN LIU[1], AND XUEFENG WANG[2]
[1]College of Electronic and Information Engineering, Changshu Institute of Technology, Changshu 215500, China
[2]College of Physics, Optoelectronics and Energy, Soochow University, Suzhou 215006, China

Corresponding author: Shuchang Wang (scw@cslg.edu.cn)

This work was supported in part by the Natural Science Foundation of Jiangsu Province under Grant BK20191027, in part by the Natural Science Research of Jiangsu Higher Education Institutions of China under Grant 18KJD510001, and in part by the Jiangsu Science and Technology Department of China under Grant BY2018203 and Grant BA2017074.

ABSTRACT In this paper, a novel resonant circuit topology is proposed for battery charging applications. Compared with traditional implemented circuits, the proposed topology can provide constant current (CC) and constant voltage (CV) charging profiles for different battery states automatically. Specially, zero-voltage-switching (ZVS) turned on of switching devices can be realized at fixed operating frequency for different charging levels, which benefits the transferring efficiency and reduces the voltage stress of the switches. In addition, simple design methodology can be derived to improve system's practicality and reliability, avoiding complex control strategy. Experimental results obtained from a 200 W prototype system show good agreement with calculated results, validating that the proposed topology can be used for battery charging systems.

INDEX TERMS Resonant converter, constant voltage, constant current, battery charging.

I. INTRODUCTION

In recent years, renewable energy and resource has attracted increased interest all over the world. As important storage elements in renewable energy systems, batteries are essential in the development of many industry applications such as consumer electronics, biomedical implants, electric vehicles (EVs) and train power supply [1]–[4]. Particularly, lithium-ion batteries are currently widely used in these applications, as a more economic type of batteries with more cycling times, compared with traditional energy storage batteries.

There are several methods utilized for charging batteries, such as taper current charging, pulse charging, reflex charging and constant voltage or current charging [5]–[10]. For taper current charging method, the current diminishes as the cell voltage builds up, which may cause a serious danger of damaging the cell if the charging rate and duration are not limited. For pulse charging method, the charging rate can be precisely controlled by varying the width of the pulses. However, the best charging duty cycle should be integrated in the controller, which makes the converter and controller complex. Among these methods, the Constant-current Constant-voltage (CC/CV) controlled charging method is the most widely used for charging Lithium and some other batteries which may be vulnerable to damage if the upper voltage and current limits are exceeded.

As shown in Fig. 1(a), the charging process contains CC mode before reaching upper voltage limit and CV mode when the current decreases to a trickle charge as the charge approaches completion [11] and [12]. Equivalent DC resistance in Fig. 1(b) can be derived from Fig. 1(a) to show the varying impedance characteristics during charging process with CCCV charging control method. The varied resistance at different charging states influences charging current, voltage and system efficiency essentially. Hence, a converter topology with simple control strategy is preferred to perform the output profiles in Fig. 1, for more reliability and practicality. In addition, the converter topology should be with high efficiency to increase energy utilization.

Battery charging technology based on DC-DC topologies has drawn attention in recent years due to its high equalization accuracy and high efficiency [13]–[18]. Mostly, control schemes for high-frequency DC-DC converters can regulate phase shift or operating frequency to adjust charging current/voltage at various load resistance [13], [14],

The associate editor coordinating the review of this manuscript and approving it for publication was Gaetano Zizzo.

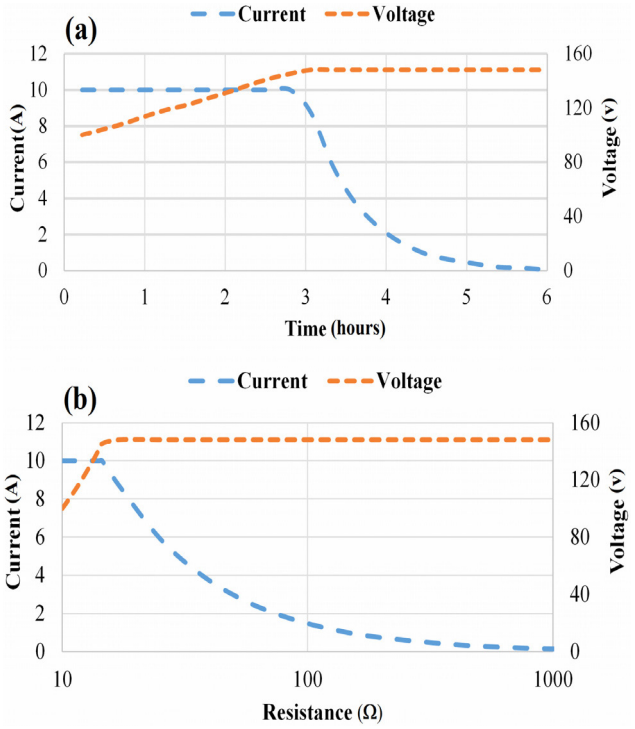

FIGURE 1. Typical CC/CV charging profile versus (a). time and (b). load resistance.

and [16]–[24]. Among proposed topologies, phase-shifted full bridge (PSFB) converters have been investigated in many aspects due to their simple structures and ZVS features. However, at light-load conditions, it is hard to maintain ZVS conditions for the lagging-leg switches, while minimize conduction loss and ringing for the secondary-side rectifier [25] and [26]. Resonant converters with frequency modulation have been proposed and researched for battery charging, such as *LLC* topology [27]–[29]. High efficiency and high power density can be achieved with *LLC* converters operating around the resonant frequency. However, it is difficult to keep high efficiency for wide output voltage range, in particular when the switching frequency is much higher or lower than the resonant frequency. In order to maintain soft-switching operation and high efficiency, many studies have been done on different modified circuit topologies or controlling methods. In [30] and [31], synchronous rectifiers (SRs) are integrated into conventional converters to obtain a higher voltage conversion ratio by controlling phase-shifted gate signals for SR switches. In [32] and [33], topologies have been proposed by transforming the structure from full-bridge to half-bridge to extend the output voltage range. However, hard switching may occur in these additional active switches for phase-shifted controlling especially at light load conditions, which leads to a lower efficiency. In order to address the hard switching problems, a variable switching-frequency control strategy for PSFB converters [34] and [35], or a phase-shift modulation method for *LLC* converters [24] and [36], are implemented under light load condition. Although higher efficiency can be obtained, the control and design methodology is relatively complex and the transition between different control modes slows down the dynamic response.

Therefore, in order to address the aforementioned issues, the paper proposed a new resonant topology for battery charging applications. The advantages of the proposed converter can be summarized as follows:

(1) ZVS turned on switching for all primary switches in different charge states;

(2) A fixed-frequency resonant operation in both CC and CV charge and hence lower circulating energy;

(3) An automatic CC/CV charging patterns without dedicated control strategies at different load resistance.

The proposed system uses a *CLCL* resonant network and two high-frequency rectifiers, connected in series at input ports and parallel at output ports. The resonant network is fed by a high-frequency converter working at fix operating frequency. A mathematical model is presented to characterize the behavior of the proposed system as well as to show how the unique characteristics can be exploited to maintain a CC or CV charging profile without requiring dedicated control regulations. Experimental results of a prototype 200W system are shown to demonstrate the validity of the proposed topology.

II. PROPOSED RESONANT CONVERTER

The proposed resonant topology, which uses a half-bridge converter, a resonant network and two identical rectifiers, is shown in Fig. 2. The *CLCL* resonant network consists of the capacitors C_i, C_t and the inductors L_i, L_t [37]. Meanwhile, the capacitor C_t is employed as DC blocking capacitor for the half-bridge converter. The input AC ports of the high-frequency rectifiers are in series, while the output DC ports are in parallel, for adding the transferred power from Part 1 and Part 2. The resistor R_L serves as a battery load with various DC resistance depending on the charging state.

The converter is operated at the desired frequency, which can be expressed as:

$$\omega_s = 2\pi f_s = \frac{1}{\sqrt{L_i C_i}} = \frac{1}{\sqrt{(L_t - \frac{1}{\omega_s^2 C_t})C_i}} \tag{1}$$

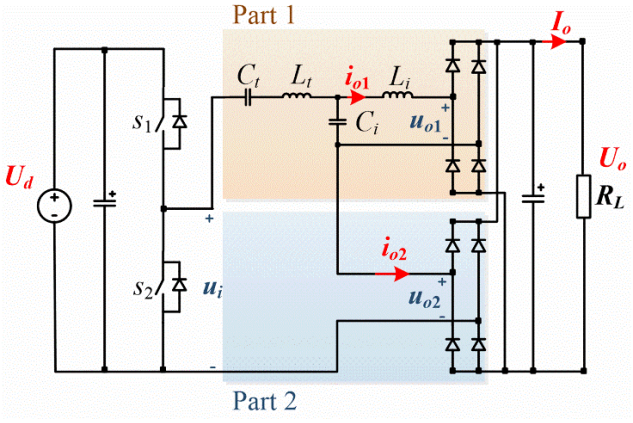

FIGURE 2. Proposed resonant converter topology.

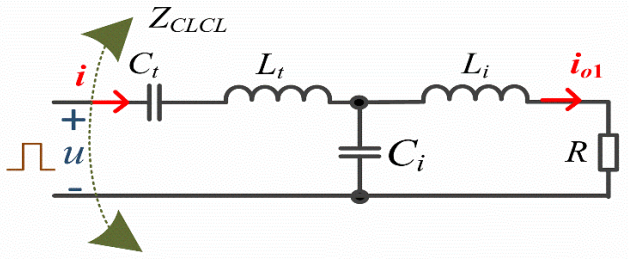

FIGURE 3. Typical circuit of CLCL network.

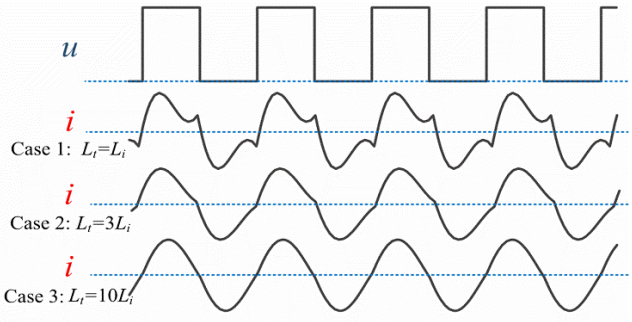

FIGURE 4. Waveforms of input voltage and current for CLCL resonant network with different L_t.

For the CLCLresonant topolog as depicted in Fig. 3, the input impedance is constantly resistanceunder tuning frequency in (1) [37], which can be expressed by:

$$Z_{CLCL} = \frac{R + j\omega_s L_i}{j\omega_s C_i R - \omega_s^2 L_i C_i} + j\omega_s L_t + \frac{1}{j\omega_s C_t} \tag{2}$$

Substituting (1) to (2), the impedance can be calculated as:

$$Z_{CLCL} = \frac{\omega_s^2 L_i^2}{R} \tag{3}$$

Meanwhile, under tuning condition as (1), the output current of the circuit in Fig. 3 can be derived as:

$$i_{o1} = \frac{u}{Z_{CLCL}} \cdot \frac{\frac{1}{j\omega_s C_i}}{\frac{1}{j\omega_s C_i} + j\omega_s L_i + R} = \frac{u}{j\omega_s L_i} \tag{4}$$

The harmonic components in input current of the *CLCL* resonant network are sensitive to the values of L_t and C_t. For example, Fig. 4 gives calculated waveforms of input current at different L_t. As can be seen, both turn-on and turn-off switching states have changed with the variations of resonant component values. Higher harmonic components may result into worse EMC performance and lower system efficiency due to high-frequency skin effect. With a resonant value of 10 L_i, Case 3 shows nearly sinusoidal current waveforms. Therefore, in order to minimize the influence by harmonic components, L_t can be larger than L_i.

The schematic diagram in Fig. 2 can be further simplified by one voltage source u_i and Z_1, Z_2 to represent impedances of Part 1 and Part 2, as shown in Fig. 5. If the value of R_L is small, the impedance Z_1 is much larger than Z_2 since L_i and C_i form a network close to parallel resonant. Therefore,

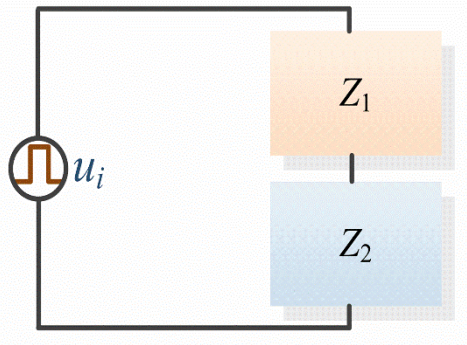

FIGURE 5. Equivalent circuit of proposed topology.

the magnitude of u_{o2} is much smaller than u_i. Fig. 6(a) shows typical waveforms during this period. As evident from (4), the output current i_{o1} is determined by the input voltage u_{o1}, performing CC state. As R_L turns to be larger, the impedance of Z_1 is decreased while Z_2 is increased. As evident from the waveforms in Fig. 6(b), both Part 1 and Part 2 transfer power to the load. Since the impedance of Z_1 and Z_2 is close to resistance, ZVS can be achieved during this period. If the load resistance becomes larger, Z_2 is much larger than Z_1, which results in large magnitude of u_{o2}, as shown in Fig. 6(c). During this period, CV performance can be achieved. In general, the proposed topology consists of two different parts, as Part 1 to perform CC characteristics (as proved by (4)) and Part 2 to perform CV characteristics. By cascading these two parts together, they can play a leading role at different load resistance as shown in Fig. 6.

It should be noted that the input voltage u_i is in phase with i_{o2}. As a result, the transferred power can be given by:

$$P_t = \frac{8}{\pi^2}(i_{o1} + i_{o2})^2 \cdot R_L = u_i \cdot i_{o2} = \frac{U_o^2}{R_L} \tag{5}$$

Under tuned condition, the current i_{o1} is determined by the input voltage of the *CLCL* network as:

$$i_{o1} = \frac{u_i - u_{o2}}{j\omega_s L_i} \tag{6}$$

The relationship of u_{o2} and the output voltage U_o, transferred by a rectifier in Part 2 shown in Fig. 2, can be determined as:

$$U_o = \frac{2\sqrt{2}}{\pi} u_{o2} \tag{7}$$

By substituting (6) and (7) into (5), the resonant current i_{o2} can be derived as:

$$i_{o2} = \frac{2M_t^2 - 2M_t\sqrt{M_t^2 - 4N_t} - 4N_t}{4R_L} \tag{8}$$

where M_t and N_t are given by:

$$M_t = \frac{\pi}{2\sqrt{2}}\sqrt{u_i}(N_t + 1) \tag{9}$$

$$N_t = \frac{R_L}{\omega_s L_i} \tag{10}$$

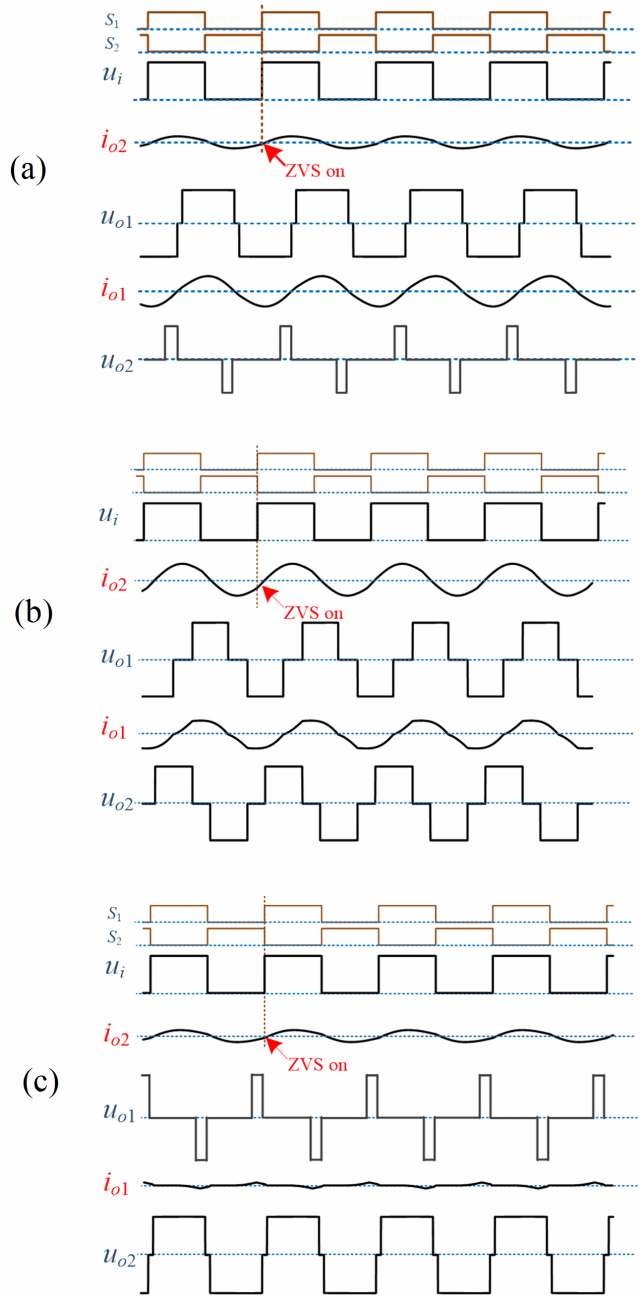

FIGURE 6. Typical waveforms of proposed topology (a). at small load resistance, (b). at middle load resistance, (c). at large load resistance.

By substituting (8)-(10) into (5), the output voltage and current can be derived as:

$$U_o = \frac{\sqrt{u_i}M_t - \sqrt{u_i M_t^2 - 4u_i N_t}}{2} \tag{11}$$

$$I_0 = \frac{\sqrt{u_i}M_t - \sqrt{u_i M_t^2 - 4u_i N_t}}{2R_L} \tag{12}$$

Equation (11) and (12) represents the relationship between the output current/voltage and the equivalent load resistance. By substituting determined resonant values into (11) and (12),

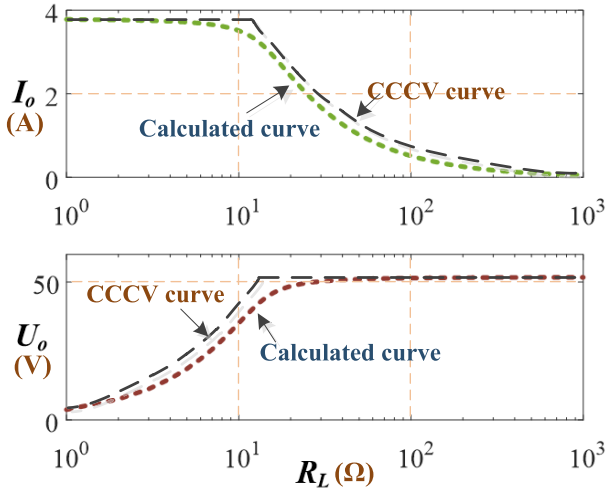

FIGURE 7. Calculated output current and voltage versus different load resistance versus CC/CV curves in Fig. 1.

variations in I_o, U_o as a function of R_L can be calculated as shown in Fig. 7, where the system was tuned at 200 kHz and the input voltage is 100 V. The resonant components C_t, L_t, C_i, L_i are designed as 10 nF, 71 μH, 80 nF and 7.9 μH. As can be seen, I_o is kept almost constant when the load resistance is less than 15 Ω. After that, U_o becomes constant while I_o decreases, as R_L is increased. Compared with the CC/CV profiles shown in Fig. 1, results in Fig. 7 indicate the output characteristics of the proposed topology is in good agreement with the trend of CC/CV curves at different load resistance. The largest difference is about 8% at the end of CC mode and the beginning of CV mode, since there is a soft transient process from CC to CV modes due to the natural feature of the proposed topology. The deviation of calculated and expected values in Fig. 7 comes from the difference between simplified fundamental analysis method at resonant frequency as shown in (1)-(12) and the nonlinear switching system.

The input voltage U_d and the resonant parameters play an important role in regulating the output power. Therefore, Fig. 8 shows variations in I_o, U_o as a function of R_L where the system was operating at different U_d and L_i. As evident from Fig. 8(a), both I_o and U_o have changed with the variations of U_d. However, increasing L_i only influences I_o under the same working conditions.

Based on above analysis, under tuning conditions in (1), the output profiles perform CC states at small load resistance and CV states at large load resistance, as can be seen in Fig. 7. The profile is coincident with characteristics of charging batteries.

Furtherly, the proposed charging topology can be converted to an isolated version with a transformer T_{r1}, as shown in Fig. 9. A DC block capacitor C_{DB} is employed to block the DC component of the voltage generated from the half-bridge converter. As can be seen, the working principle is the same as discussed before. Efficiency is a little lower than the proposed topology in Fig. 2, because of the high-frequency transformer. However, the output voltage and current values can be adjusted by changing the turn ratio of the transformer.

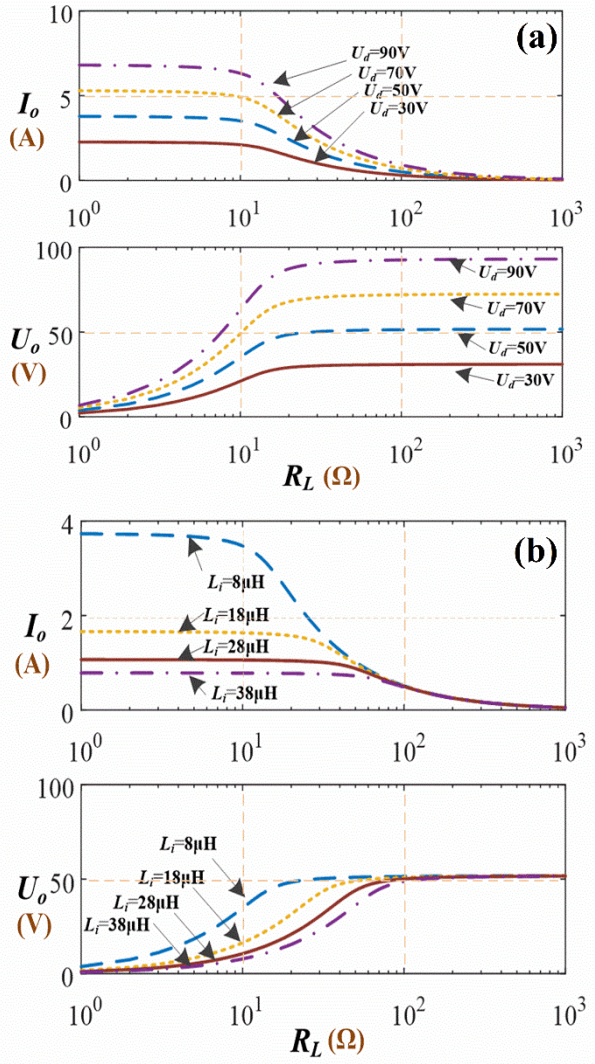

FIGURE 8. Calculated output current and voltage versus load resistance with (a). different input voltage and (b). different inductors L_i.

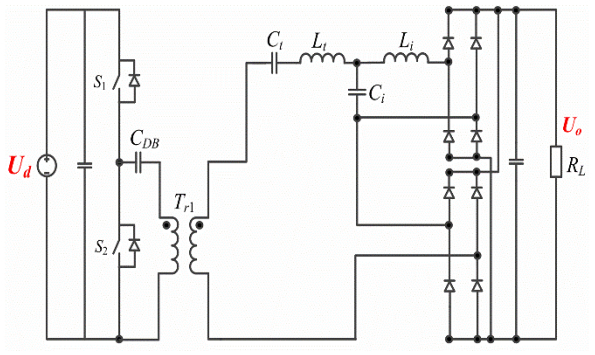

FIGURE 9. Schematic diagram of isolated version of proposed topology.

Compared with traditional PSFB or *LLC* converters, ZVS switching can be obtained easily without dedicated controllers or additional active switches, which can benefit the system design and increase the reliability. The drawback of the proposed topology is the extra rectifier, which may increase the cost of the system. However, from another view, more distributed diodes may benefit the design of cooling system especially at high transferred power level.

III. EXPERIMENTAL RESULTS AND DISCUSSIONS

A resonant system with the circuit in Fig. 2 was designed and built to validate the viability of the proposed topology, as shown in Fig. 10. The system comprises a 200 W converter and two high-frequency rectifiers, which were connected by a *CLCL* network. Fig. 11 illustrates the steps to design the system parameters. Firstly, the CC and CV values and the resonant frequency should be determined. For charging batteries, the CC charging value is usually specified from manufacturers as the maximum charging rate which the battery can be fully charged while avoiding damaging by overcharging. Meanwhile, the CV charging value should be predetermined according to the battery cell upper voltage limit, which is known as the float level during the CV mode. After selecting specific batteries, the U_o, I_o can be determined firstly. The optimum switching frequency is found on the basis of design tradeoffs amongst converter's efficiency, size, weight and cost. Higher frequencies may produce smaller solution size using lower valued resonant inductors and capacitors, but decrease efficiency and impact thermal performance with higher magnetic core and copper losses in passive resonant elements. In this design, the switching frequency is selected as 100 kHz for the switching device IPP200N25N3G.

As shown in Fig. 5 and Fig. 6, if the load resistance R_L is very small, the impedance Z_1 is much larger than Z_2 as can be seen in (3), Fig. 6 and Fig. 7. Therefore, the CC current value can be simplistically determined as shown in (4). According to the selected switching frequency, L_i is calculated as:

$$L_i = \frac{u}{j\omega_s i_o} = \frac{\frac{\sqrt{2}U_d}{\pi}}{j\omega_s(\frac{\pi}{2\sqrt{2}}I_o)} = 35.8\mu\text{H} \tag{13}$$

Thus, a close resonant inductor L_i is selected as 33.4 μH due to dead-time effect of half-bridge converter.

As a result, the resonant capacitor C_i can be calculated as 75.8 nF by (1). An approximate value 74.2 nF is achieved by combinations of several resonant capacitors shown in Fig. 10.

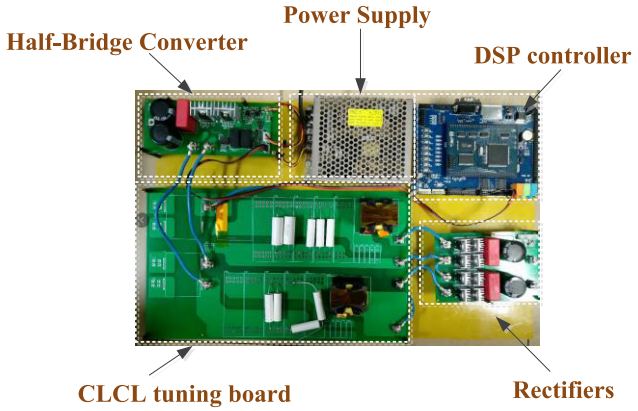

FIGURE 10. Experiment setup.

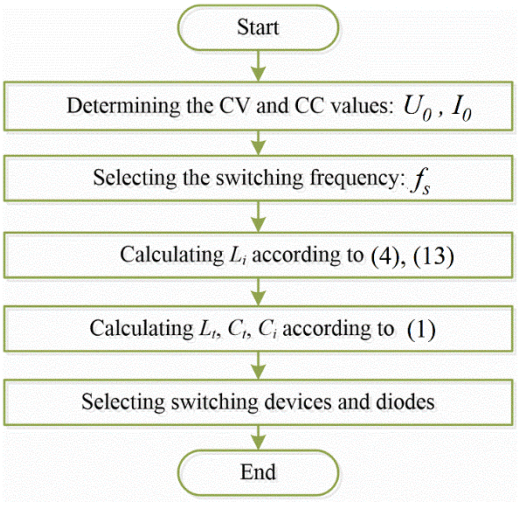

FIGURE 11. Design steps of system parameters.

TABLE 1. Parameters of experimental setup.

C_t	25 nF
L_t	135.2 μH
C_i	74.2 nF
L_i	33.4 μH
f_s	100 kHz
U_{in}	200 V
C_o	40 μF
MOS	IPP200N25N3G
Diode	C3D10060A
CC value I_o	3.6 A
CV value U_o	100 V

According to Fig. 4, the inductor L_t is determined as much larger than L_i to minimize the influence by harmonic components. Here, L_t is determined as 135.2 μH, as $4L_i$ to eliminate the harmonics in current. Substituting L_t into (1), C_t is derived as 24.8 nF. As a result, a capacitor of 25 nF is selected into the resonant topology.

If the load resistance R_L is large, the impedance Z_2 is much larger than Z_1 as shown in Section II, thus Part 2 plays the most important role in these conditions, which means the CV value U_o is determined as:

$$U_o = \frac{2\sqrt{2}}{\pi} u_{o2} = \frac{2\sqrt{2}}{\pi} \cdot \left(\frac{\pi}{4\sqrt{2}} U_d \right) = \frac{U_d}{2} \qquad (14)$$

Thus, the input voltage U_d is derived as 200 V. The parameters of the prototype are given in Table 1.

The experimental results of output voltage and current are compared with the calculated values, as shown in Fig. 12. When the load resistance is less than 28 Ω, the output current decreases slowly, while the output voltage increases markedly. After that, the output voltage keeps almost constant and the output current decreases dramatically. Both the simulated and experimental results are in good agreement, confirming the accuracy of the calculated model.

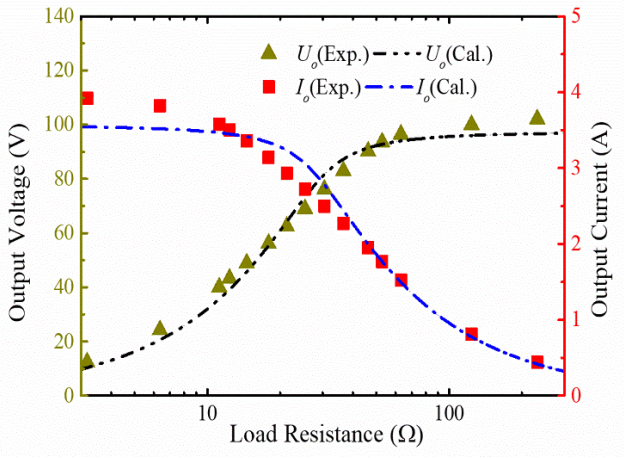

FIGURE 12. Experimental and calculated results of output current and voltage with different load resistance.

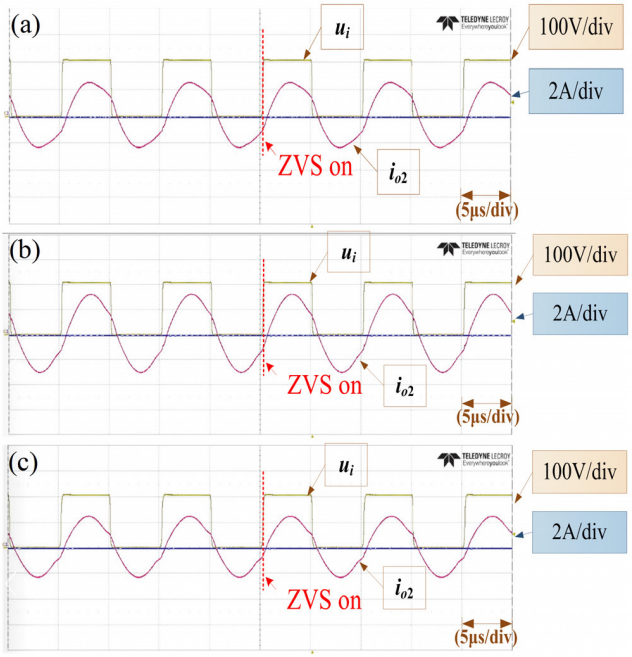

FIGURE 13. Experimental waveforms of u_i, i_{o2}, i_{o1} for different load resistance. (a) R_L = 12.6 Ω, (b). R_L = 32.1 Ω, (c). R_L = 65 Ω.

According to the analysis presented in Section II, the relative phase between u_i and i_{o2} is not influenced by the variations in the load resistance. Thus, the experimental waveforms taken from the prototype, where R_L is 12.6 Ω, 32.1 Ω, and 65 Ω, are shown in Fig. 13. As evident from the results, the phase between u_i and i_{o2} is almost zero with the increased resistance. The magnitude of i_{o2} increases firstly, then decreases. As a result, ZVS of the switching devices can be realized at fixed operating frequency for different load resistance, which means under tuning conditions in (1), the output profiles perform CC states at small load resistance and CV states at large load resistance as shown in Fig. 12. As a result, the performance of the proposed topology is coincident with characteristics of charging batteries.

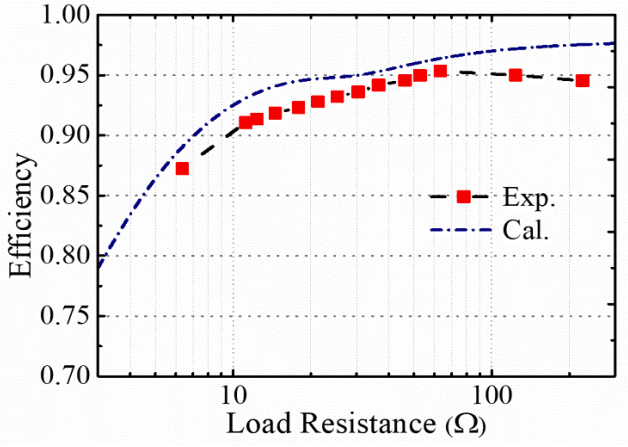

FIGURE 14. Experimental and calculated results of system efficiency with different load resistance.

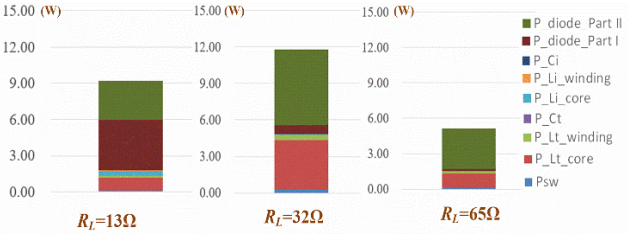

FIGURE 15. Loss distributions at different load resistance.

The total efficiency was measured with different load resistance as shown in Fig. 14. As evident from the results, the efficiency changes slightly for CV charging state, while the efficiency increases for CC charging state because the losses of diodes account for a larger proportion for low voltage and high current charging state. The peak efficiency of the system is 95.4%.

In order to illustrate the efficiency performance at different load resistance, Fig. 15 gives the loss distributions for different operating conditions. When R_L is 13 Ω for CC charging state, the diode losses in Part 1 in Fig. 2 accounts for the largest proportion of the total losses. As R_L becomes larger, the diodes loss in Part 2 takes larger proportion. Meanwhile, the core losses in the inductor L_t increases first and then decreases obviously, as the load resistance is increased. It should be noted that the switching losses P_{sw} is relatively very small owing to the ZVS switching performance.

To sum up, the benefits of the proposed resonant topology are as follows:

(1) The experimental current i_{o2} and voltage u_i of the designed converter indicate that ZVS turn on for all primary switches can be achieved during both CC and CV charge states at different load resistance. Thereby, the efficiency of the proposed resonant converter is promoted, especially with light load.

(2) The switching frequency is fixed and closed to the resonant frequency, which is beneficial for transferring efficiency and reducing the voltage stress of the switches.

TABLE 2. Comparison between proposed topology and existing works.

Case	Efficiency	Switching Frequency Range	System Complexity
Proposed topology	high	small	low
LLC [16]-[24]	high	large	low
PSFB [13] and [14]	medium	small	low
PSFB with frequency modulation [34] and [35]	medium	small	high
LLC with phase-shift modulation [24] and [36]	high	medium	high

(3) No dedicated control strategy is utilized for CC/CV output characteristics, which can improve the system reliability and practicality.

In general, a comparison between the proposed topology and existing works has been listed in Table 2, to shown the advantages of the new topology as discussed above.

IV. CONCLUSION

A novel resonant converter topology has been proposed for battery charging applications. The proposed topology utilizes a *CLCL* resonant network and two high-frequency rectifiers to realize CC or CV charging states with different load resistance automatically, without a dedicated sophisticated controller. ZVS turn on can be achieved for all switches in the proposed converter, which benefits the transferring efficiency and voltage stress. The novel resonant circuit has been described in detail and calculated to show the unique characteristic of power transfer. Experimental results of a prototype 200 W system have been presented to demonstrate the applicability of the proposed converter.

REFERENCES

[1] S. Hild, S. Leavey, C. Graf, and B. Sorazu, "Smart charging technologies for portable electronic devices," *IEEE Trans. Smart Grid*, vol. 5, no. 1, pp. 328–336, Jan. 2014.

[2] G. Bum Joun and B. H. Cho, "An energy transmission system for an artificial heart using leakage inductance compensation of transcutaneous transformer," *IEEE Trans. Power Electron.*, vol. 13, no. 6, pp. 1013–1022, Nov. 1998.

[3] A. F. Burke, "Batteries and ultracapacitors for electric, hybrid, and fuel cell vehicles," *Proc. IEEE*, vol. 95, no. 4, pp. 806–820, Apr. 2007.

[4] W. Su, H. Eichi, W. Zeng, and M.-Y. Chow, "A survey on the electrification of transportation in a smart grid environment," *IEEE Trans Ind. Informat.*, vol. 8, no. 1, pp. 1–10, Feb. 2012.

[5] E. Ayoub and N. Karami, "Review on the charging techniques of a li-ion battery," in *Proc. 3rd Int. Conf. Technological Adv. Electr., Electron. Comput. Eng. (TAEECE)*, Apr. 2015, pp. 50–55.

[6] V. Prajapati, H. Hess, E. J. William, V. Gupta, M. Huff, M. Manic, F. Rufus, A. Thakker, and J. Govar, "A literature review of state of-charge estimation techniques applicable to lithium poly-carbon monoflouride (LI/CFx) battery," in *Proc. India Int. Conf. Power Electron. (IICPE)*, Jan. 2011, pp. 1–8.

[7] V. V. Dimitrov, P. T. Goranov, and D. S. Hvarchilkov, "Methods and power converters for charging/formation of VRLA batteries," in *Proc. 26th Int. Scientific Conf. Electron. (ET)*, Sep. 2017, pp. 1–4.

[8] H. A. Serhan and E. M. Ahmed, "Effect of the different charging techniques on battery life-time: Review," in *Proc. Int. Conf. Innov. Trends Comput. Eng. (ITCE)*, Feb. 2018, pp. 421–426.

[9] W. Sutopo, M. Nizam, B. Rahmawatie, and F. Fahma, "A review of electric vehicles charging standard development: Study case in Indonesia," in *Proc. 5th Int. Conf. Electric Veh. Technol. (ICEVT)*, Oct. 2018, pp. 152–157.
[10] Y. Gao, X. Zhang, Q. Cheng, B. Guo, and J. Yang, "Classification and review of the charging strategies for commercial lithium-ion batteries," *IEEE Access*, vol. 7, pp. 43511–43524, 2019.
[11] G. Buja, M. Bertoluzzo, and K. N. Mude, "Design and experimentation of WPT charger for electric city car," *IEEE Trans. Ind. Electron.*, vol. 62, no. 12, pp. 7436–7447, Dec. 2015.
[12] D. H. Tran, V. B. Vu, and W. Choi, "Design of a high-efficiency wireless power transfer system with intermediate coils for the on-board chargers of electric vehicles," *IEEE Trans. Power Electron.*, vol. 33, no. 1, pp. 175–187, Jan. 2018.
[13] H. Wang and Z. Li, "A PWM LLC type resonant converter adapted to wide output range in PEV charging applications," *IEEE Trans. Power Electron.*, vol. 33, no. 5, pp. 3791–3801, May 2018.
[14] V. R. K. Kanamarlapudi, B. Wang, P. L. So, and Z. Wang, "Analysis, design, and implementation of an APWM ZVZCS full-bridge DC–DC converter for battery charging in electric vehicles," *IEEE Trans. Power Electron.*, vol. 32, no. 8, pp. 6145–6160, Aug. 2017.
[15] N. Tashakor, E. Farjah, and T. Ghanbari, "A bidirectional battery charger with modular integrated charge equalization circuit," *IEEE Trans. Power Electron.*, vol. 32, no. 3, pp. 2133–2145, Mar. 2017.
[16] Z. Zhao, Q. Xu, Y. Dai, and A. Luo, "Minimum resonant capacitor design of high-power LLC resonant converter for comprehensive efficiency improvement in battery charging application," *IET Power Electron.*, vol. 11, no. 11, pp. 1866–1874, Sep. 2018.
[17] Z. Li, T. Wu, G. Zhang, and R. Yang, "Hybrid modulation method combining variable frequency and double phase-shift for a 10 kW LLC resonant converter," *IET Power Electron.*, vol. 11, no. 13, pp. 2161–2169, Nov. 2018.
[18] C. Zhang, Z. Gao, and X. Liao, "Bidirectional DC–DC converter with series-connected resonant tanks to realise soft switching," *IET Power Electron.*, vol. 11, no. 12, pp. 2029–2043, Oct. 2018.
[19] B.-Y. Chen and Y.-S. Lai, "Switching control technique of Phase-Shift-Controlled full-bridge converter to improve efficiency under light-load and standby conditions without additional auxiliary components," *IEEE Trans. Power Electron.*, vol. 25, no. 4, pp. 1001–1012, Apr. 2010.
[20] V. Kinnares and P. Hothongkham, "Circuit analysis and modeling of a phase-shifted pulsewidth modulation full-bridge-inverter-fed ozone generator with constant applied electrode voltage," *IEEE Trans. Power Electron.*, vol. 25, no. 7, pp. 1739–1752, Jul. 2010.
[21] R. Beiranvand, B. Rashidian, M. R. Zolghadri, and S. M. H. Alavi, "Using LLC resonant converter for designing wide-range voltage source," *IEEE Trans. Ind. Electron.*, vol. 58, no. 5, pp. 1746–1756, May 2011.
[22] F. Musavi, M. Craciun, D. S. Gautam, W. Eberle, and W. G. Dunford, "An LLC resonant DC–DC converter for wide output voltage range battery charging applications," *IEEE Trans. Power Electron.*, vol. 28, no. 12, pp. 5437–5445, Dec. 2013.
[23] R. Beiranvand, B. Rashidian, M. R. Zolghadri, and S. M. H. Alavi, "Optimizing the normalized dead-time and maximum switching frequency of a Wide-Adjustable-Range LLC resonant converter," *IEEE Trans. Power Electron.*, vol. 26, no. 2, pp. 462–472, Feb. 2011.
[24] Y.-K. Lo, C.-Y. Lin, M.-T. Hsieh, and C.-Y. Lin, "Phase-shifted full-bridge series-resonant DC-DC converters for wide load variations," *IEEE Trans. Ind. Electron.*, vol. 58, no. 6, pp. 2572–2575, Jun. 2011.
[25] Y. Jang, M. M. Jovanovic, and Y. M. Chang, "A new PWM ZVS full-bridge converter," *IEEE Trans. Power Electron.*, vol. 18, no. 5, pp. 1122–1129, Sep. 2003.
[26] G.-B. Koo, G.-W. Moon, and M.-J. Youn, "New zero-voltage-switching phase-shift full-bridge converter with low conduction losses," *IEEE Trans. Ind. Electron.*, vol. 52, no. 1, pp. 228–235, Feb. 2005.
[27] B. Yang, F. C. Lee, A. J. Zhang, and G. Huang, "LLC resonant converter for front end DC/DC conversion," in *Proc. 17th Annu. IEEE Appl. Power Electron. Conf. Exposit. (APEC)*, Mar. 2002, pp. 1108–1112.
[28] D. Fu, B. Lu, and F. C. Lee, "1 MHz high efficiency LLC resonant converters with synchronous rectifier," in *Proc. IEEE Power Electron. Spec. Conf.*, Jun. 2007, pp. 2404–2410.
[29] X. Xie, J. Zhang, C. Zhao, Z. Zhao, and Z. Qian, "Analysis and optimization of LLC resonant converter with a novel over-current protection circuit," *IEEE Trans. Power Electron.*, vol. 22, no. 2, pp. 435–443, Mar. 2007.
[30] J.-W. Kim and G.-W. Moon, "A new LLC series resonant converter with a narrow switching frequency variation and reduced conduction losses," *IEEE Trans. Power Electron.*, vol. 29, no. 8, pp. 4278–4287, Aug. 2014.
[31] D. Fu, Y. Liu, F. C. Lee, and M. Xu, "A novel driving scheme for synchronous rectifiers in LLC resonant converters," *IEEE Trans. Power Electron.*, vol. 24, no. 5, pp. 1321–1329, May 2009.
[32] H. Hu, X. Fang, F. Chen, Z. J. Shen, and I. Batarseh, "A modified high-efficiency LLC converter with two transformers for wide input-voltage range applications," *IEEE Trans. Power Electron.*, vol. 28, no. 4, pp. 1946–1960, Apr. 2013.
[33] X. Sun, X. Li, Y. Shen, B. Wang, and X. Guo, "Dual-bridge LLC resonant converter with fixed-frequency PWM control for wide input applications," *IEEE Trans. Power Electron.*, vol. 32, no. 1, pp. 69–80, Jan. 2017.
[34] Z. Lei, L. Haoyu, W. Chao, and L. Yuan, "A method of optimizing the switching frequency based on the loss analysis model," in *Proc. 40th Annu. Conf. IEEE Ind. Electron. Soc. (IECON)*, Oct. 2014, pp. 4103–4109.
[35] A. Mallik and A. Khaligh, "Variable-switching-frequency state-feedback control of a phase-shifted full-bridge DC/DC converter," *IEEE Trans. Power Electron.*, vol. 32, no. 8, pp. 6523–6531, Aug. 2017.
[36] H. Wu, T. Mu, X. Gao, and Y. Xing, "A secondary-side phase-shift-controlled LLC resonant converter with reduced conduction loss at normal operation for hold-up time compensation application," *IEEE Trans. Power Electron.*, vol. 30, no. 10, pp. 5352–5357, Oct. 2015.
[37] D. J. Thrimawithana and U. K. Madawala, "A generalized steady-state model for bidirectional IPT systems," *IEEE Trans. Power Electron.*, vol. 28, no. 10, pp. 4681–4689, Oct. 2013.

SHUCHANG WANG received the Ph.D. degree from the School of Electronic Science and Engineering, Southeast University, Nanjing, China, in 2015. Since 2019, he has been a Postdoctoral Research Fellow with Soochow University, Suzhou, China. He is currently a Teacher with the College of Electronic and Information Engineering, Changshu Institute of Technology, Changshu, China. His current research interests include simulation calculation and design of power devices.

YUSHEN LIU received the Ph.D. degree from the Department of physics, Fudan University, Shanghai, China, in 2007.

From 2008 to 2010, he was a Postdoctoral Research Fellow with National Chiao Tung University, Taiwan, China. Since 2009, he has been an Assistant Professor with the Physics Department, Indiana State University, Indiana, USA. He is currently a Professor with the College of Electronic and Information Engineering, Changshu Institute of Technology, Changshu, China. He is the author of more than 80 articles. His research interests include nano-electronics process and device design.

XUEFENG WANG received the Ph.D. degree in semiconductor device physics from the Shanghai Institute of Microsystem and Information Technology (SIMIT), Chinese Academy of Sciences (CAS), Shanghai, China, in 1994.

From 1995 to 2001, he was a Postdoctoral Research Fellow with Rio State University, Rio de Janeiro, Brazil. From 2001 to 2006, he was an Associate Research Fellow with Concordia University and the University of Manitoba, Canada. From 2007 to 2009, he was a Senior Scientist with Atomistix (Asia Pacific) Company, Singapore. He is currently a Professor with the College of Physics, Optoelectronics and Energy, Soochow University, Suzhou, China. His research interests include the simulation calculation and design of semiconductor devices.